Walter, T. R., Motagh, M. (2014): Deflation and inflation of a large magma body beneath Uturuncu volcano, Bolivia? Insights from InSAR data, surface lineaments and stress modelling. - *Geophysical Journal International*, *198*, 1, p. 462-473

DOI: http://doi.org/10.1093/gji/ggu080

Geophysical Journal International

Geophys. J. Int. (2014) **198,** 462–473
Advance Access publication 2014 May 23
GJI Geodynamics and tectonics

doi: 10.1093/gji/ggu080

Deflation and inflation of a large magma body beneath Uturuncu volcano, Bolivia? Insights from InSAR data, surface lineaments and stress modelling

Thomas R. Walter and Mahdi Motagh

*GFZ German Research Centre for Geosciences, Telegraphenberg, D-*14473 *Potsdam, Germany. E-mail: twalter@gfz-potsdam.de*

Accepted 2014 March 4. Received 2014 March 4; in original form 2013 July 2

SUMMARY

The voluminous ash-flow eruptive products in the Central Andes imply that there are major magma bodies; however, how these magma bodies develop and change in time and space are not understood. In this study, we analyse the deformation activity of the Uturuncu Volcano, SW Bolivia, from 2003 to 2009 using a satellite radar interferometry (InSAR) data set. We find that the strength and the pattern of the present deformation can be explained by a pressurized source, such as an inflating flat-topped magma body at ∼22 ± 9 km depth below the surface. Furthermore, we examine the optical remote sensing data to perform a lineament analysis, which shows in a geographic information system (GIS) that a girdle of river streams and faults encircle the volcano at radial distance of approximately 15 km. Using numerical stress models, we locate a magma body beneath the volcano and find that the lineaments are best explained by a deflating flat-topped magma body at approximately 18 ± 2 km depth, which is consistent with the InSAR study. Thus, both the independent analysis of InSAR and lineament data suggest the presence of a horizontally extended, flat-topped magma body beneath Uturuncu. The location depth is in agreement with, or just above, a prominent seismic low velocity zone. Consequently, although the sign of deformation caused by the herein constrained magma body differs, the similar geometry and similar location suggest them to be similar, possibly indicating longevity of a magma storage region.

Key words: Magma chamber processes; Remote sensing of volcanoes; Volcano monitoring.

1 INTRODUCTION

The knowledge about the geometry and the extent of ancient and exposed large crustal magma bodies is foremost constrained by geology and often complemented by geochemical, geophysical and modelling approaches (Walker 1989; Gudmundsson 2012). The available field data of old, eroded magma chambers, which are known as plutons, suggest that these chambers have a common tabular (flat-topped)-shaped geometry with low aspect ratios that often resembles a sill-shaped magma body (Marsh 2000; Gudmundsson 2012). However, geophysical data alone cannot conclusively determine the presence, the shapes and the dimensions of large magma bodies. Geodetic data, for instance, are often explained by assuming infinitely small pressurized points and prolate or oblate volumes (Dzurisin 2007), which simplifies or even opposes the geological knowledge on reservoirs' geometric and dynamic complexities (Bott & Smithson 1967; Pitcher 1979).

Probably most magma chambers develop from sills (Gudmundsson 2012), governed by the internal and external stress fields, periodicities of repeated intrusions, roof collapse and crustal assimilation, often developing into flat-topped magma chamber roofs (Marsh 1982). However, the evolution duration of large magma chambers remains unclear; conceptual models vary from near instantaneous magma emplacement and short magma chamber life spans to the emplacement by multiple pulses and intermittent injections of magma over millions of years (Bergantz 2000; Petford *et al.* 2000).

At the surface, large developing reservoirs are thought to be associated with updoming of the crust, which may serve as an initial stage of an eruption and thus has received rigorous attention in terms of volcano activity monitoring and hazard assessment (Dzurisin 2007). In some cases, cauldrons and calderas may develop, associated with significant drainage of such magma bodies. Here we report on a system that may display signs of both inflation and deflation. The question was, if the same reservoir can explain these different deformations.

We utilize remote sensing data to constrain and validate the shape of a reservoir by exploiting two different approaches: a radar

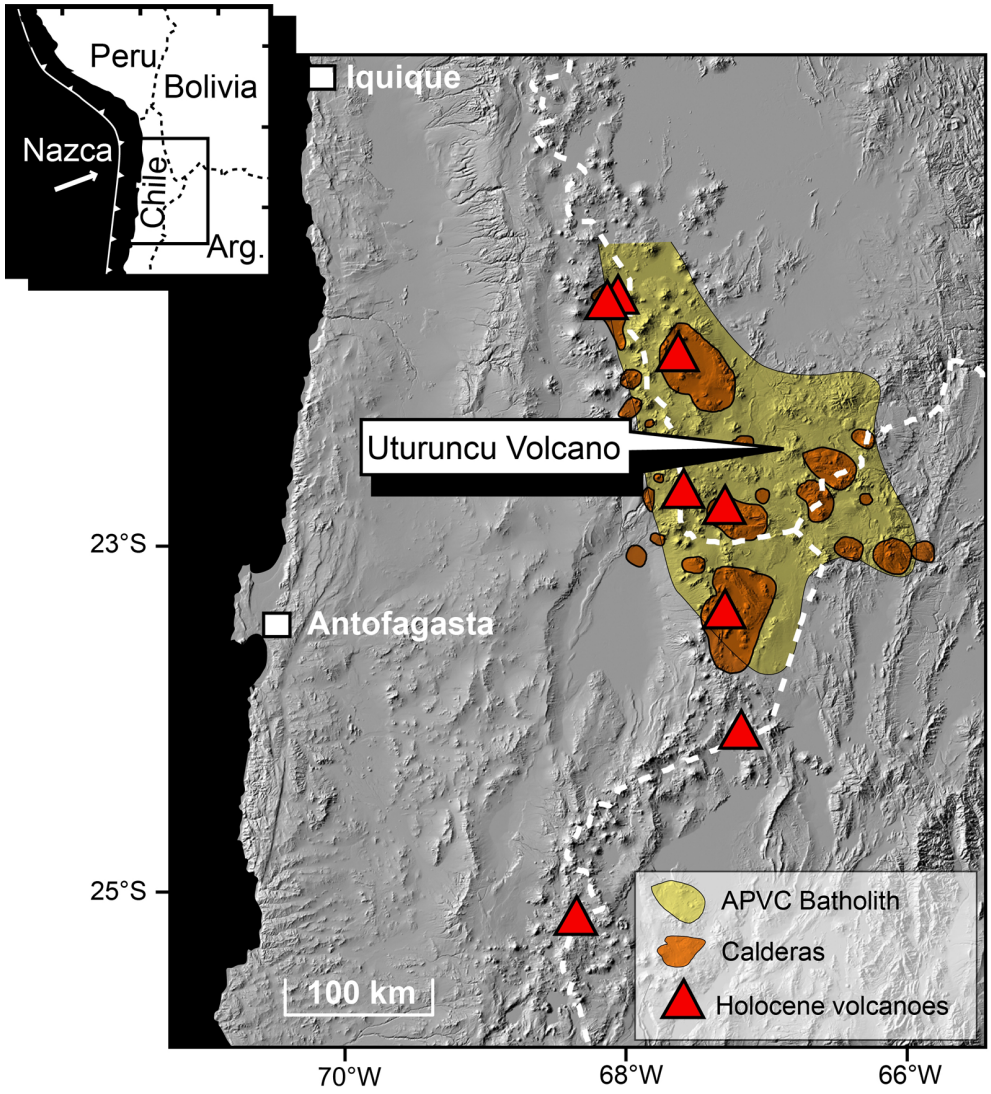

Figure 1. Shaded relief map showing the location of historically active volcanoes (red triangles), the extended APVC batholith area (yellow shading) and calderas (auburn shading) after (de Silva & Gosnold 2007). Holocene volcanoes shown by red triangles.

geodetic approach that focuses on current, short-term, deformation activity and a geographic information system approach (GIS) that focuses on structural mapping of geological features.

Our study area is located in the central Andes, which is known for its large-scale caldera systems (de Silva *et al.* 2006). Between 21°S and 25°S, eight such systems have had historically recorded eruptions (Fig. 1). As constrained by satellite radar interferometry, some deforming areas suggest magmatic inflation at locations without historical eruptions or otherwise much attention in the past century (Pritchard *et al.* 2002). The largest deforming area is located in the southwestern part of Bolivia at the historically inactive Uturuncu volcano and provides a rare showcase example of a large-scale magma body emplacement and the associated deformation.

2 STUDY AREA: UTURUNCU VOLCANO

Volcanism in the Central Andes is related to the subduction of the Nazca Oceanic Plate under the South American Plate (Allmendinger *et al.* 1997). There is evidence of large-scale and voluminous intrusions and explosive volcanism (Fig. 1); the latter is particularly well preserved in the form of ignimbrite deposits in the Altiplano Puna Volcanic Complex (APVC; de Silva *et al.* 2006). The APVC is located between 21°S and 25°S and is related to several crustal intrusion bodies, many of which are sill-like and evident from high electrical conductivity, gravity and seismic tomography studies (see Oncken *et al.* (2006) and refs. therein). Catastrophic eruptions from the APVC are associated with the development of major calderas. A 400-km-long seismic reflection profile (ANCORP) revealed the presence of a large scale low-velocity zone located at a depth of ∼18 km below sea level (ANCORP Working Group 2003). This ultralow velocity zone (ULVZ) is assumed to be relatively thin, possibly less than 1 km, but extending laterally under the APVC for at least 100 km (Chmielowski *et al.* 1999; Leidig & Zandt 2003; Zandt *et al.* 2003). The ULVZ is according to these studies the magma source for many eruptions in the region.

In the elevated region (>3800 m) of the Altiplano, the volcanoes of southwestern Bolivia and their products have been deposited on a 70-km-thick crust, which hosts the upper crustal magma storage system (Zandt *et al.* 2003). The basement is partially composed of folded and faulted mid-Miocene rocks and provides a pronounced

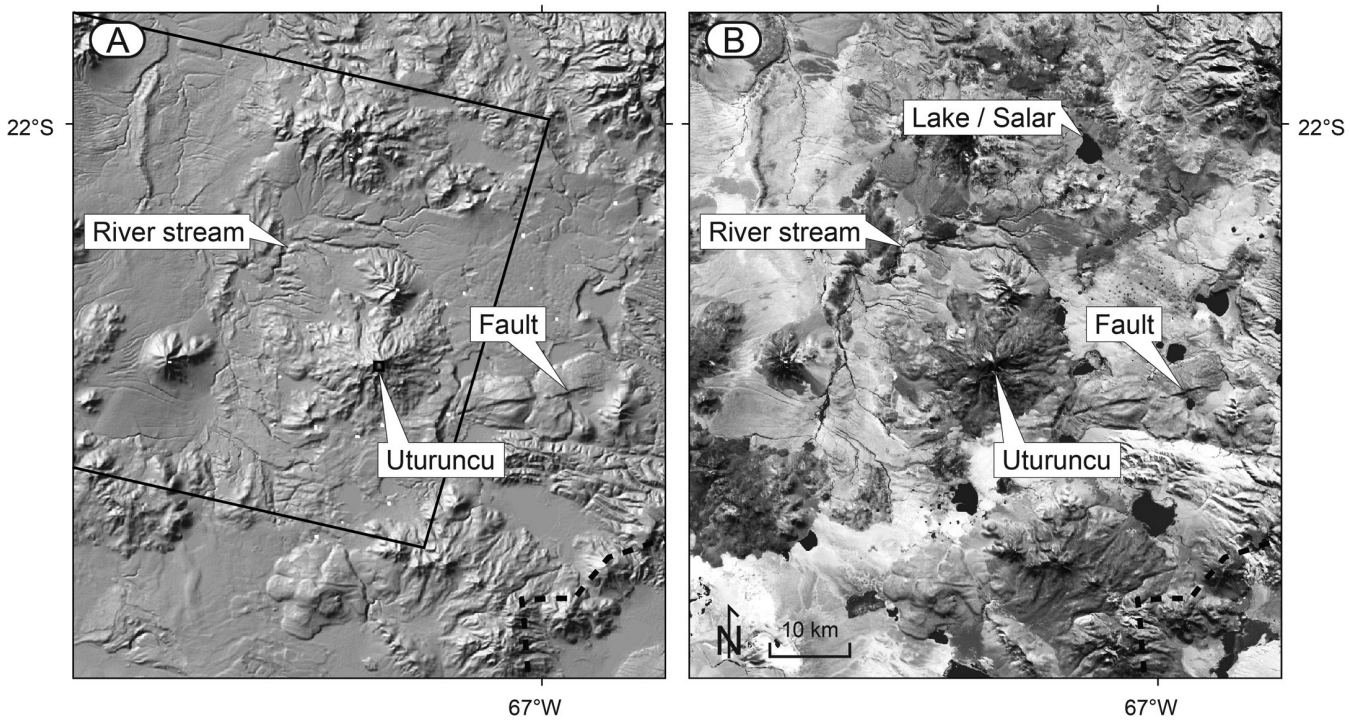

Figure 2. Three-arcsec digital elevation model (A) and Landsat TM image (channel 7, B) show Uturuncu volcano in the centre, river streams, lakes or salars (in black) and fault strikes. Uturuncu volcano is seen as a steep stratovolcano with dark lava flows. Black box in left-hand image shows outline of descending ENVISAT radar image frame (track 282).

regional tectonic lineament pattern (de Silva & Francis 1991; Riller & Oncken 2003). Locally, the lineaments appear distorted by additional processes such as magmatic loading as discussed below.

Located in the southwestern part of Bolivia, the Uturuncu volcano is a dominant morphological peak (area 400 km^2, elevation ~6000 m at 22.27°S, 67.18°W). Its activity has been related to minor degassing and low-temperature fumaroles. Thus, this notably remote area received minor scientific and public interest. However, in the last several years, Uturuncu has received much scientific interest mainly because it is recognized as one of the largest updoming volcanic zones by area on Earth (Pritchard & Simons 2002, 2004; Pritchard *et al.* 2002; Sparks *et al.* 2008; Jay *et al.* 2012).

The volcanic products of Uturuncu are Pleistocene dacite lavas and domes (Fig. 2); even the youngest summit lavas are excessively abraded by glaciers (de Silva & Francis 1991). Age dating suggests that the span of volcanic activity around Uturuncu is approximately 10–15 Ma, which was overlain by lava flows 0.9–0.5 Ma, and the present summit lava dome 0.27 Ma (Sparks *et al.* 2008). Thus, field and remote sensing data could not provide any evidence of an eruptive activity in the past 270 000 yr at the Uturuncu volcano; however these data may only represent an extended dormant period. Deformation detected by interferometric processing of satellite radar data (InSAR) suggest that an area of over 1000 km^2 is uplifting at an annual peak rate of 10 mm, which affects the Uturuncu volcano and the surrounding plains (Pritchard *et al.* 2002; Pritchard & Simons 2004) but gradually decreases with time (Fialko & Pearse 2012).

These earlier InSAR studies used both the standard two-pass differential InSAR technique (e.g. Pritchard & Simons 2004), or advanced time-series methods that rely on a larger data set (e.g. Fialko & Pearse 2012) to show a pronounced large-scale doming region. Simple elastic modelling could explain this inflation pattern by magma bodies of different shapes at various intrusion depths (Pritchard *et al.* 2002; Pritchard & Simons 2004; Jay *et al.* 2012). Some modelling studies results may indicate that the pressure changes at depth (Hickey *et al.* 2013). Other studies suggest a diapir-like ascent in connection to a much larger mid-crustal ULVZ (Fialko & Pearse 2012).

It is well known that the model simulations that best reproduce the observed deformation strongly depend on the model assumptions made and appear non-unique. Therefore, according to the above studies that apply elastic material conditions, the same deformation at Uturuncu can be explained assuming pressurized point sources, penny-shaped cracks, sill-shaped reservoirs or spherical (prolate or oblate) geometries at various depths and strengths, all of which can fit the data in the noise level, although the location depths may differ by 50 per cent or more (*cf.* Pritchard & Simons 2004). In other words, the inferred depth of the magma source ranges from 12 km below sea level for a finite crack to approximately 17 km for spherical chambers and 25 km for a point crack (Pritchard *et al.* 2002; Pritchard & Simons 2004; Jay *et al.* 2012). Especially if deformation data from the near field is considered only (Shirzaei & Walter 2009), both the depth and the geometry of the source causing the deformation often remains unclear, which is why additional constraints are required.

3 DATA AND RESULTS

In this study, we combine two independent approaches to explain the observed local structural architecture and improve the knowledge of the deformation source. We first re-investigate the satellite data and create a time-series to analyse the recent deformation pattern at Uturuncu. This InSAR-related work does not re-analyse the full available InSAR data set, as completed in (Fialko & Pearse 2012). Instead, we aim to provide a robust InSAR data set and a model base to compare with our new GIS lineament investigations. The

InSAR-data derived deformation source is modelled based on different assumptions, to confirm the results by Pritchard *et al.* that the solutions at Uturuncu cover a broad range of reservoir shapes and locations. Then, we perform a GIS investigation that focuses on characterization of lineaments, that is, dominant strikes of morphology caused by faults, folds, lakes, rivers and streams. We construct numerical stress field models to better understand the formation pattern of the structure-related lineaments based on the Coulomb fracture criterion.

3.1 InSAR time-series analysis

By performing an InSAR time-series analysis, we map the space–time evolution of the deformation signal at Uturuncu. Radar images of the study area are acquired using the European Space Agency's ENVISAT spacecraft. The data set consists of 25 ASAR images that were recorded in a descending orbit (track 282) between 2003 March and 2009 March.

To derive the time-dependent surface deformation from this data set, we follow a two-step process. First, using the DORIS software (http://doris.tudelft.nl) with the 90-m SRTM DEM and the precise orbits provided by ESA, we form a coherent network of temporally overlapped interferograms. The interferograms are processed using a multi-looking factor of 4 pixels in range and 20 pixels in the azimuthal direction, which results in a resolution of 80 m for the interferometric products. We subsequently identify in each interferogram a subset of multi-looked pixels whose coherence were above a threshold of 0.25 and estimate the time-series of the displacement using a least-square inversion technique (Berardino *et al.* 2002; Usai *et al.* 2003), as implemented in the software package StaMPS/MTI (Hooper 2008).

Fig. 3 shows the estimated mean uplift rate in the radar line-of-sight (LOS) at Uturuncu for 2003–2009. The results show an inflating area of ∼40 km in diameter with a maximum rate of 5 ± 1 mm yr^{-1}. A recently identified large wavelength moat surrounding the inflation area with a 150 km diameter (Fialko & Pearse 2012) is beyond the image space shown in here. The lower panel in Fig. 3 shows two InSAR time-series examples. Point 1 lies inside the main deformation field, and its time-series exhibits a clear positive trend of ∼5 mm yr^{-1}, which is possibly related to the volcanic process under Uturuncu. Point 2 is outside the main deformation area and shows no significant deformation in time. The results generally reveal uplift at Uturuncu, which is consistent with previous two-pass InSAR (Pritchard *et al.* 2002; Pritchard & Simons 2004) and more recent InSAR time-series analyses (Sparks *et al.* 2008; Fialko & Pearse 2012). An oscillatory behaviour in time (Fig. 3) may occur because of the atmospheric effect or the transient deformation, the latter resembles a seasonal variation. However, because the 'stable point' also shows a somewhat comparable oscillation, a concluding interpretation of this oscillation without ground truth validation is beyond the scope of this work and has not been further analysed.

To obtain information about the source of deformation, we model the previously derived average uplift rate signal using various magma reservoir geometries in a linear elastic half-space. We consider a Mogi point source (Mogi 1958), a Penny-shaped crack (Fialko *et al.* 2001) and a sill-shaped intrusion (Okada 1992). For the inversion, we resample the average velocity signal at Uturuncu to a 500 m grid and solve for the best-fitting volcano deformation source using a nonlinear inversion approach (Faeghlashgary *et al.* 2012).

The results are shown in Fig. 4. For the point-source inversions, the results suggest a location at 25 ± 4 km depth (Table 1), in

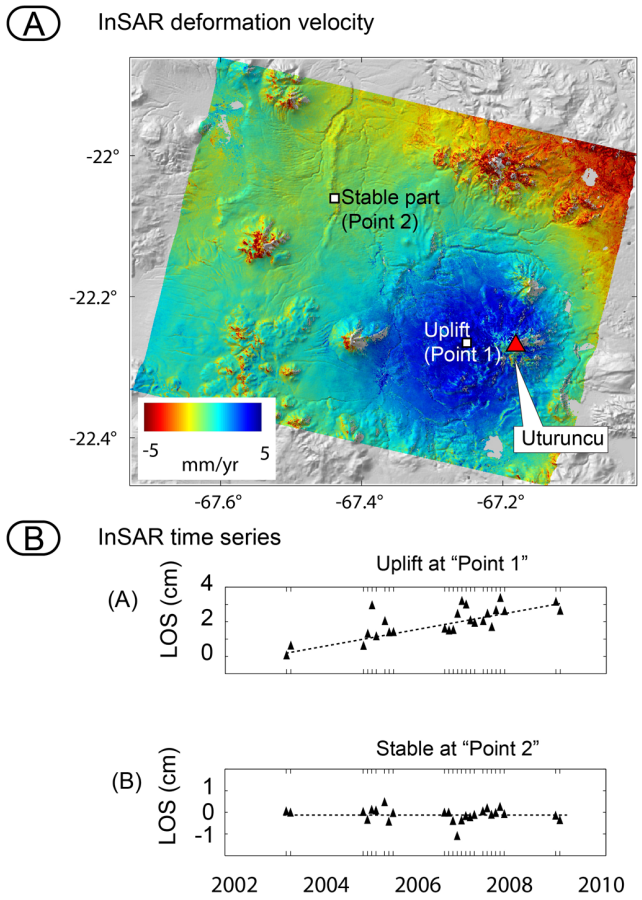

Figure 3. InSAR time-series results show the spatial and temporal pattern of the deformation zone. Note that the site of maximum uplift, shown in blue colours, is slightly offset to the west with respect to the Uturuncu volcano. Deformation trend was found to be roughly linear and the stable area was found to be located outside the deformation region. Reddish colours to the northeast of Uturuncu appear in mountainous regions and were not further investigated herein.

agreement with (Henderson & Pritchard 2013). These values are also comparable to the previous observations using InSAR and modelling in a different data period (Pritchard *et al.* 2002; Pritchard & Simons 2004). However, if another source geometry is used, then these numbers change considerably. Constraining the source shape to be horizontally extended like a flat-topped magma body or the roof of a larger diapir-shaped magma chamber (Yun *et al.* 2006), we obtain a depth of $\sim 22 \pm 9$ km below the surface. The depth range roughly agrees with the position of the low velocity zone underneath the region (Zandt *et al.* 2003). Although the InSAR data display the deformations in details, they do not allow us to uniquely identify the shape and the position of a potential magma reservoir roof. Therefore, we add the GIS results as described in the following section. The limitations of the models and the assumptions are further analysed in the discussion section.

3.2 GIS study

3.2.1 Lineaments

Lineaments are known as lines in the landscape that are associated with the hidden architecture of the rock basement (Hobbs 1904). Lineaments are commonly described as mappable features, which

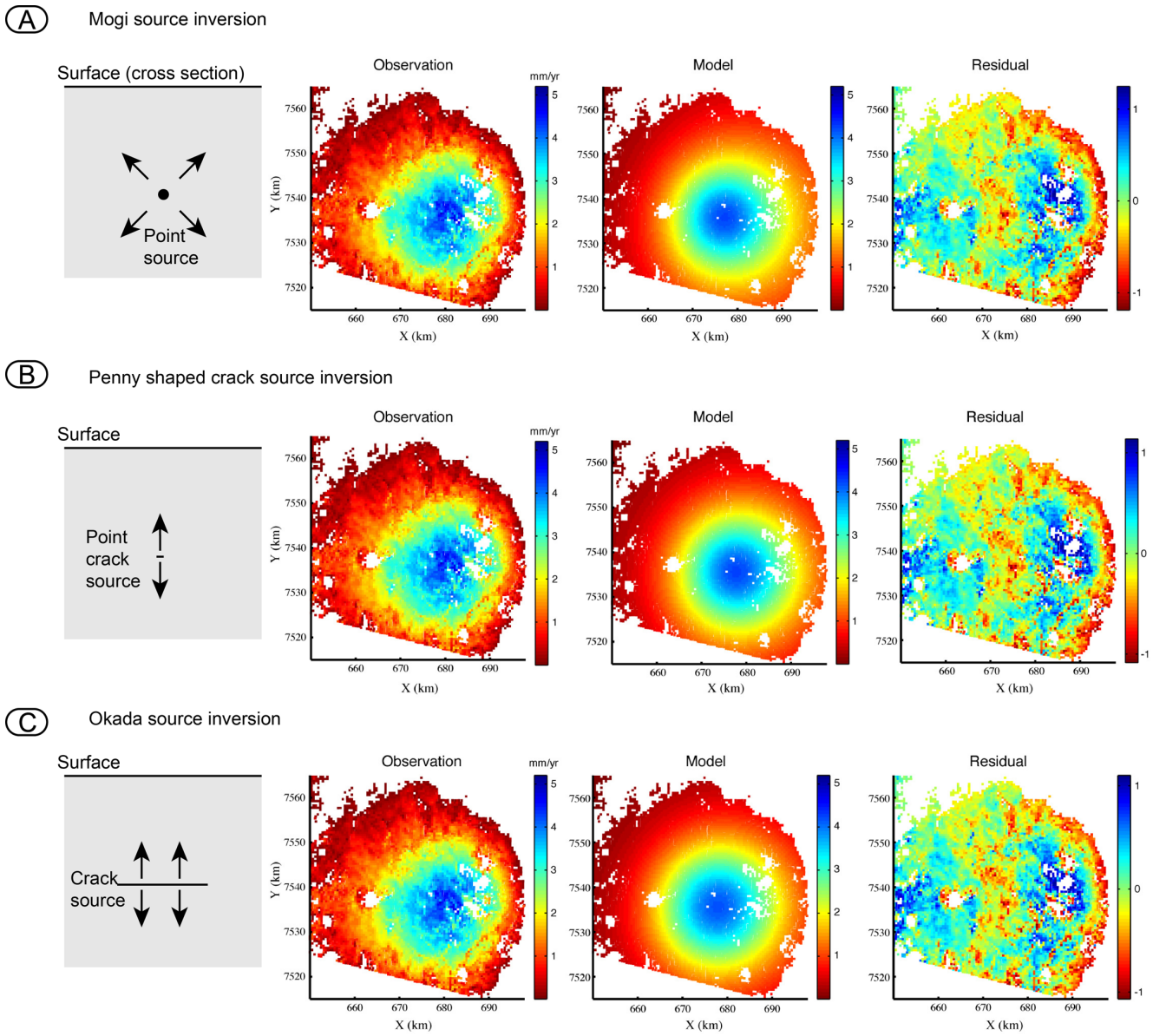

Figure 4. Inversion of deformation signal at Uturuncu based on commonly used analytical formulations, from top to bottom: a Mogi point source (Mogi 1958), a Penny-shape crack (Fialko *et al.* 2001) and finally a rectangular-shaped intrusion (Okada 1992). Illustration of residuals show that all these considered model geometries reproduce the signal similarly well.

Table 1. Inversion results for three different source types (Mogi, Penny and Okada) for the uplift rate signal at Uturuncu. For the Okada model the ratio between length and width was assumed to be 1 and the dip angle was fixed to zero in the inversion so as to simulate a near-horizontal plane of a flat-topped reservoir.

Model	Depth of the source beneath surface
Mogi	21 ± 6
Okada	22 ± 9
Penny	29 ± 6

are often linear and presumably reflect the subsurface phenomena (O'Leary *et al.* 1976). Remote sensing data augmenting studies on lineaments, which are found as linear lines and edges determined by spatial-domain filtering techniques on colorized pixels, have become increasingly available (Soto-Pinto *et al.* 2012). The mapped lineaments may result from different geomorphological and geological processes such as rivers, valleys, ridges, faults and fractures. Traditionally, lineaments are associated with long-term processes, but there is increasing evidence that even short time spans may produce or activate new lineament systems such as the ones that occurred after earthquakes (Arellano-Baeza *et al.* 2006). Lineaments that are expressed as topographic lows are commonly associated with joints, faults and shear zones underground, whereas the lineaments that are expressed as topographic highs are interpreted as dykes and dyke swarms (Ramli *et al.* 2010). Because of the correlation between lineaments and structures in the field, lineaments represent fracture networks (Morelli & Piana 2006).

The surroundings of Uturuncu are breached by abundant morphological and structural lineaments (Fig. 5), which we investigated using remote sensing data and geoinformatic techniques. Landsat TM (bands 1–7), aerial photographs and 3 arcsec shuttle radar

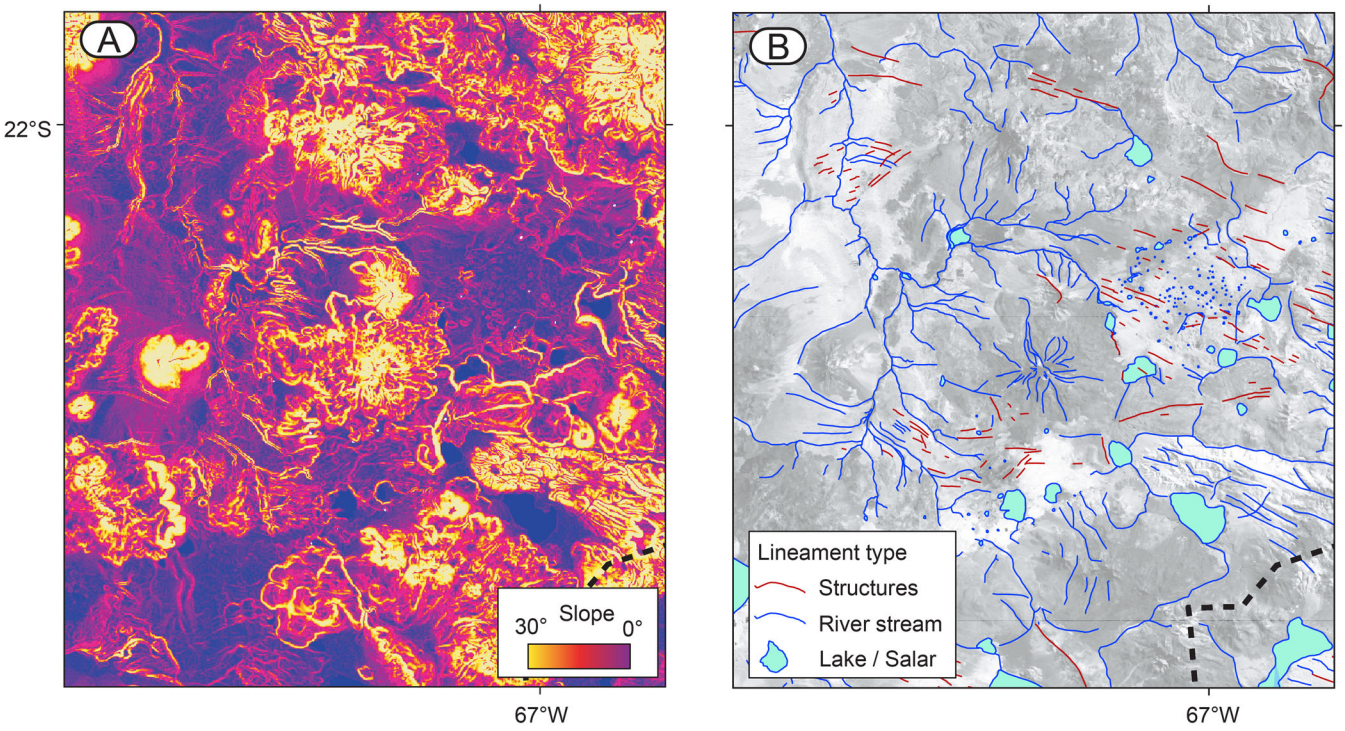

Figure 5. (A) Lineaments identified in slope maps and satellite images. (B) Lineaments were digitized and categorized into three classes.

topography data were imported and georeferenced in ArcGIS. The lineaments were digitized in a radius of 100 km with respect to the Uturuncu summit and classified into (i) structural lineaments, that is, faults and folds that were clearly distinguishable from the data, (ii) fluviatile and river lineaments that were characterized by deep morphological erosion patterns, (iii) outlines of salars and lakes and (iv) all other lineaments that could not be attributed to one of the aforementioned classes. To account for the length and weight of the lineaments, we partition each of it into 100-m-long sublineaments, that is, a 1-km-long fault lineament contains 10 sublineaments. For each sublineament, we calculated the centre and the endpoint locations and the azimuthal direction. The azimuths were statistically visualized and further analysed in rose diagrams. The rose diagrams are illustrated in three classes, that is, rivers/streams and faults/folds and the outlines of lakes, salt lakes (salars) and volcanic morphology (as measured at half of the volcano height). We performed the analysis for the (arbitrarily defined) far-field, that is, lineaments located at 50–100 km radial distance from the Uturuncu centre (Fig. 6), and the near-field, that is, lineaments located within 50 km from the volcano (Fig. 7).

The analysed far-field lineaments contain 1087 volcano morphology sublineaments trending N101° ± 17° (95 per cent confidence interval), 5463 river lineaments trending N125° ± 6° and 1457 structural sublineaments trending N108° ± 3° (Fig. 6). Thus, the far-field trend is consistently striking in the WNW–ESE direction and resembles the orientation of major tectonic faults and basement structures that are identified elsewhere in the region (de Silva 1989). A possible local effect associated with a long-wavelength moat associated to a diapir-like magma body (Fialko & Pearse 2012) could not be identified by our lineament study.

The near-field lineaments (Fig. 7) are first shown using their numbers in a lineament density map (calculation parameters: cell size 0.005°, search radius 0.05°). The mapping results of the lineaments suggest a zone of fractures surrounding the Uturuncu volcano. This

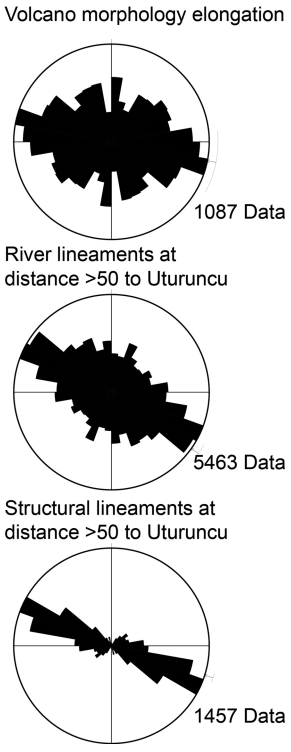

Figure 6. Lineament azimuths far away from Uturuncu are plotted in rose diagrams and suggest predominant WNW–ESE strikes.

inferred *fracture girdle* is subcircular with a maximum detectable diameter of 51 km and a peak-to-peak value of 28 km. The rose diagrams, which are presented in five geographic sectors, therefore show a significantly different situation from the far-field data. We observed in the northeastern sector N128° ± 17°, the northwestern

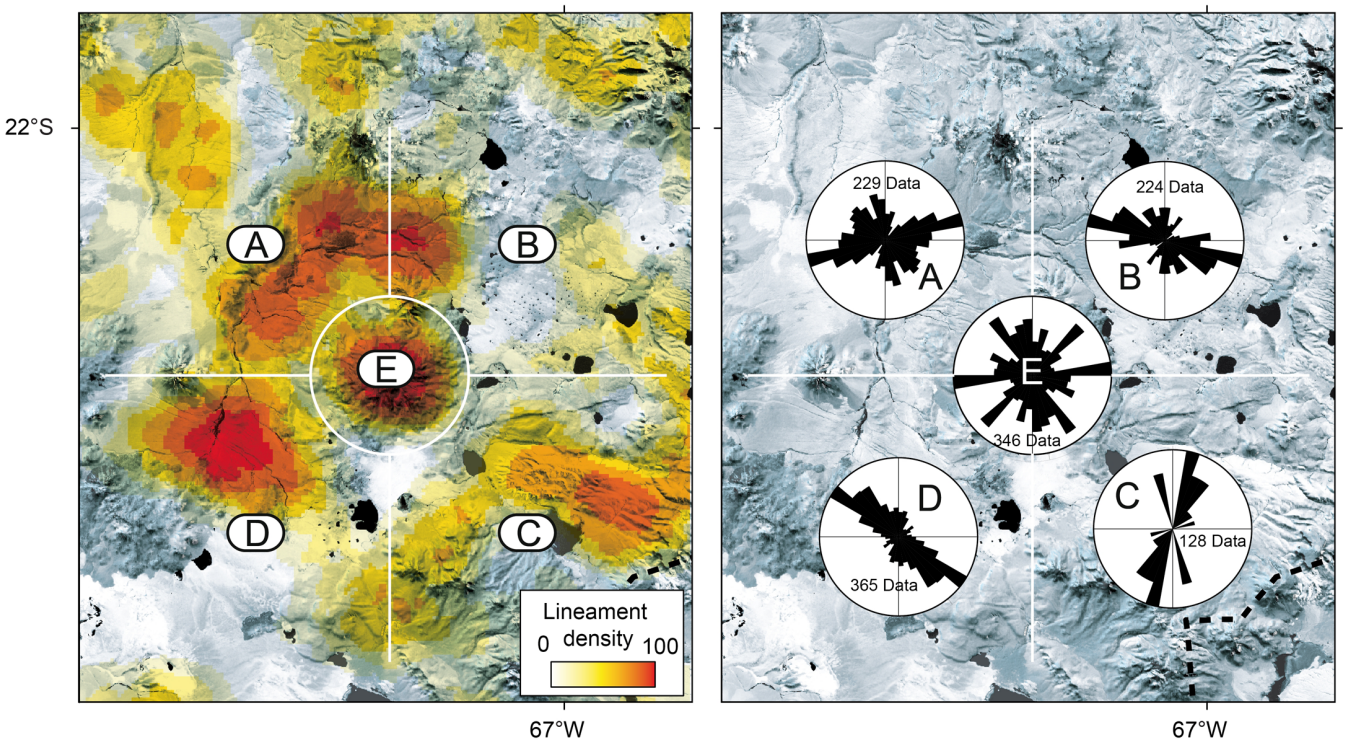

Figure 7. Lineament density (left-hand panel) and lineament azimuths (right-hand panel) close to Uturuncu. Density map suggests a girdle of lineaments surrounding Uturuncu volcano (search radius of 0.05°, output cell size of 0.005°); rose diagrams shown in four sectors (A, B, C and D) and in the centre (E) suggest a circumferential strike direction that markedly differs from the regional pattern shown in Fig. 6.

sector N101° ± 36°, the southwestern sector N141° ± 10° and in the southeastern sector N025° ± 19°. Thus, the rose diagrams of the four sectors surrounding the Uturuncu volcano suggest a different strike from the far-field strike, which approximates a circumferential azimuth with respect to the volcano centre. The lineaments on the volcano centre are interpreted to occur mainly because of slope erosion; thus they are radially oriented and do not have a deep-seated structural origin.

3.2.2 Stress models based on lineaments

Lineaments may form for many reasons. Lineaments may develop in episodes or anytime during the geological history. If the lineaments are associated to deformations, then they can be examined by palaeostress analysis. As summarized in Section 3.2.1, lineaments are commonly thought to be associated with faults and fractures. Conjecturing that the bulk lineament pattern surrounding Uturuncu volcano is structural in origin, the reconstruction of the palaeostress field requires knowledge or assumptions on the type of structures. Lineaments associated with thrust, normal or strike-slip kinematics result in different interpretations.

In a simplistic view, thrust faults may form when the minimum compressive stress σ_3 is vertical, normal faults may form when the maximum compressive stress σ_1 is vertical and strike-slip faulting may form when the vertical principal stress is intermediate (Anderson 1951). Ideally conjugate shear fractures are observed by lineaments, allowing detailed analysis on the principal stress axes. In such a conjugate system, earlier studies (Hancock & Al-Kadhi 1978) showed that σ_1 bisects the smallest dihedral angle whilst σ_2 is oriented parallel to the intersection of the two conjugate fractures. As a result, the orientation of the three major stress directions can be accurately determined. However, in this study we could not observe such conjugate systems at Uturuncu. Alternatively, the condition to form an extension fracture might be given, which is controlled by the tensile stress condition, so that the occurrence and spacing of tension lineaments can be used to estimate the responsible amplitude of the stress. In solid mechanics, fracture experiments show that fracture initiation depends on the differential stress and on the maximum horizontal tensile stress near the surface (Twiss & Moores 1992). Thus, the Uturuncu fracture girdle may represent the pattern of the maximum tensile stress. No actual displacements by lithology offsets or topographic throws could be observed by us at the lineament locations, supporting our interpretation. Whether faults, for example, normal faults, really exist at depth remains speculative, which is why we concentrate our analysis on the tensile stress field near the surface.

To explore the majority of the fractures using the maximum-tensile-stress pattern, we designed 3-D boundary element models (Thomas 1993). The code uses triangular dislocations and calculates the elastic fields from the solution for the angular dislocation in the elastic half-space (see also (Walter 2007)). For the magma body source, we consider a spherical, oblate or prolate chamber of variable dimensions, locations and aspect ratios and we calculate the tensile stress at the surface (Fig. 8).

The forward inflation model simulations suggest that the maximum tensile stress at the surface occurs directly above the inflating magma body. The high-tensile-stress region is local with a high amplitude for prolate and spherical sources, whereas it is wide and with a lower amplitude for flat-topped (e.g. sill-shaped) sources. The deflation models also show a centralized maximum tensile stress above the chamber for prolate and spherical sources. For the deflating flat-topped magma chambers, we observe a ring of maximum tensile stress at the surface that generally encircles the lateral edges of the magma chamber beneath. Hence, a flat-topped magma body is the

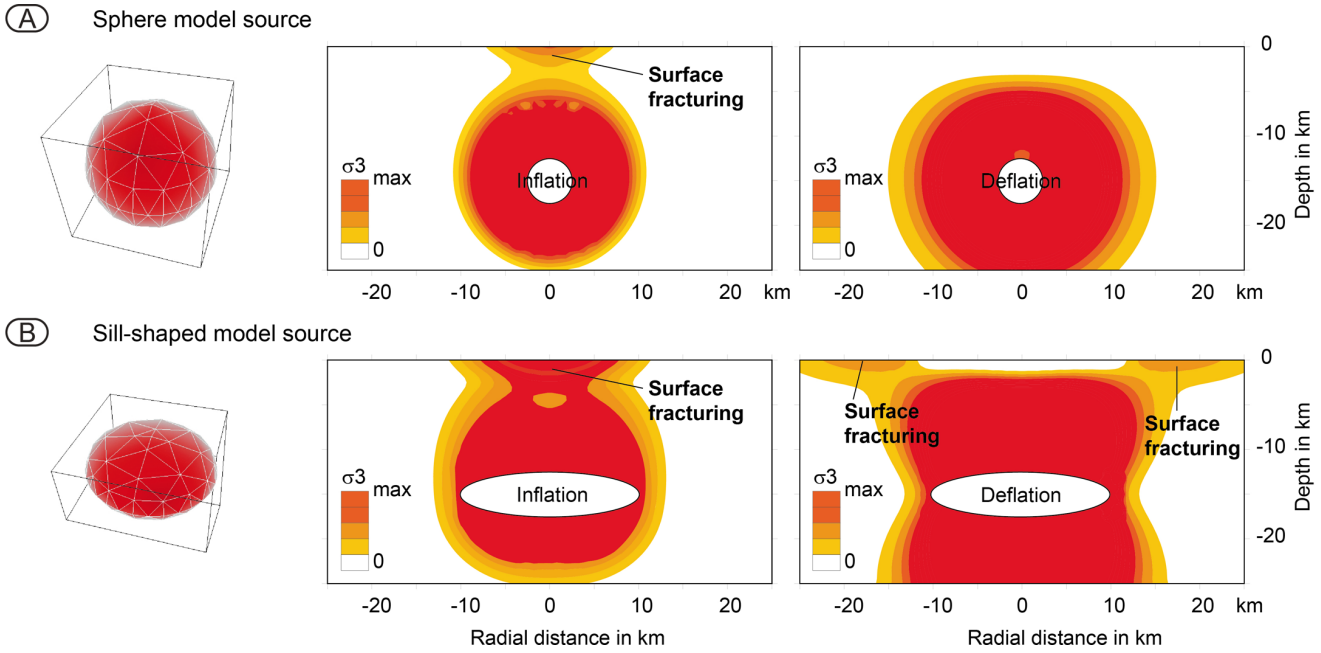

Figure 8. Boundary element model setup examples (left-hand panel) and tensile stress calculations for inflation (middle row) and deflation (right-hand panel) magma chamber. Here for illustration only two geometries are shown, a spherical chamber (A) and an oblate-shaped chamber (B). Note that a deflating oblate-shaped chamber, that is, the flat-topped chamber, is producing a ring of maximum tensile stress at the surface.

most plausible source geometry to display a ring of tensile stress and may explain the observed girdle of fractures at the surface.

To account for the 28 km diameter of the fracture girdle peak (Fig. 7), using a grid search approach, we find that the flat-topped magma chamber must be 18 ± 2 km deep. The stress field calculation is consistent with the lineament appearance (Fig. 9). The suggested depth range is consistent with the previously described independent InSAR data analysis, and also with the location of the prominent seismic low-velocity zone.

4 DISCUSSION

Voluminous ignimbrite deposits and large caldera basins suggest the presence and the periodic flares of extended magma bodies (de Silva & Gosnold 2007). Here we analysed Uturuncu, the largest actively deforming volcano area known in the Andes (Pritchard *et al.* 2002; Pritchard & Simons 2004; Sparks *et al.* 2008; Fialko & Pearse 2012; Jay *et al.* 2012). By InSAR data analysis, as well as the Landsat data, the aerial images and the shuttle radar topographic data, we determine and investigate the types and pattern of lineaments, and compare to the displacement maps.

The local lineaments at Uturuncu differ from the far-field WNW–ESE trend, which suggests the significant influence of a local deformation source. The strike and the spacing of the lineaments show a girdle surrounding the Uturuncu volcano at radial distances of 16–51 km. Because of this radial symmetry, we assume that a local process causes this pattern. Using numerical models, we tested if this local process might be related to a pressurized source at depth. We investigate the inflation and deflation of sources with various shapes under the surface, and calculate the maximum tensile stress at the surface. A girdle of high maximum tensile stress is found for deflating flat-topped magma source. The spatial dimensions of this stress girdle is similar to the observed lineaments if the source is located at the ∼18 ± 2 km depth below the surface. Remarkably, a similar depth is also constrained by independent data, as we inverted the line-of-sight displacements of InSAR data, which yield a flat-topped source at the 22 ± 9 km depth below the surface. However, the strength and the sign of this geodetically constrained source is the opposite of those for the lineament-derived source: the lineaments imply deflation, whereas the InSAR data imply inflation.

4.1 Implications

4.1.1 Shape

In a unifying model, the deformation, the lineament analysis and the stress modelling suggest a flat-topped source at Uturuncu. As emphasized in this work, and demonstrated in earlier studies (Yun *et al.* 2006), the 3-D shape of a magma body and its geometry beneath the deformation source can hardly be determined from near field geodetic data alone. The deformation is characteristically dominated by the roof region of a magma body and approximated by models (Dzurisin 2007). Therefore, the shape of the flat-topped source is not in conflict with the recent finding that the far-field deformation pattern of Uturuncu is related to a diapir-shaped source (Fialko & Pearse 2012). The diapirs roof may be flat-topped instead of being convexly bended. Alternative source constellations and interpretations are summarized in Henderson & Pritchard (2013).

4.1.2 Depth

The depth range characterized by our work is consistent with other data. A zone of high electrical conductivity, gravity and seismic anomaly is thought to occur because of a crustal zone of partial melt and magma intrusions (Schmitz *et al.* 1997; Chmielowski *et al.* 1999), with a seismic velocity that approaches only 1 km s^{-1} at depths of 17–19 km below sea level (Leidig & Zandt 2003; Zandt *et al.* 2003). The reservoirs constrained by InSAR and the lineament study may represent a localized region in this Altiplano-Puna ULVZ.

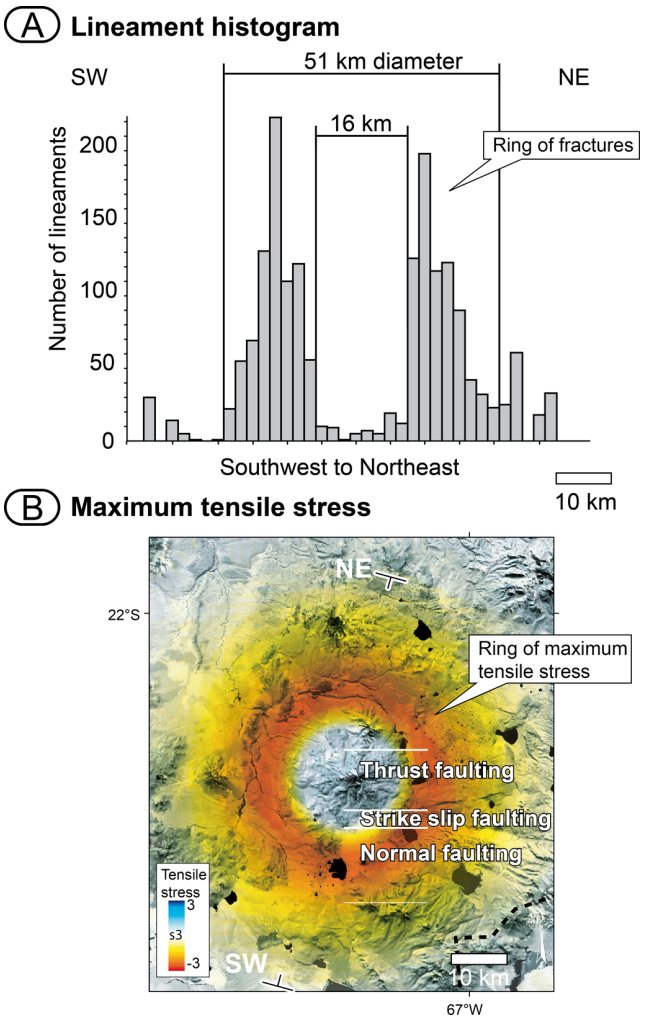

Figure 9. (A) Histogram along a 10 km wide SW–NE profile with projected cumulative lineaments at 2 km bins showing two main peaks 16–51 km in diameter, describing a ring of fractures. (B) Boundary element model suggesting a ring of maximum tensile stress (σ_3) used to explain the location and width of the fracture ring. The only source type found able to produce such a ring resembles a deflating flat-toped intrusion at 13–31 km depth.

Local anomalies in this ULVZ (Leidig & Zandt 2003; Zandt *et al.* 2003) may lead to volcanic activity and unrest. Possibly, the Uturuncu magma body is not the only active magma body under the Altiplano-Puna plateau, as suggested by gravity data modelling (Hickey *et al.* 2013). If the interpretation of the presence of local anomalies and magma uprise within the Altiplano-Puna ULVZ is correct (Fialko & Pearse 2012), our study suggests that such anomalies may be flat topped and may exist for considerable time and (temporally) even reverse the sign.

4.1.3 The moat(s) of Uturuncu

The fracture ring locates in a moat, that is, in an area that by altitude is relatively low if compared to the surrounding (Fig. 10). The diameter of the fracture ring is ∼51 km, with a radial distance of the maxima to Uturuncu of 14 km (Fig. 8). Another moat was identified with a diameter of ∼150 km and therefore at a much larger radial distance to the Uturuncu uplift region (Fialko & Pearse 2012; Henderson & Pritchard 2013). These two moats are not to be confused. While the local moat and fracture girdle is interpreted by us to be related to the flat-topped roof of a reservoir, the large scale moat at distance is likely due to viscous flow associated with the diapir rise of magma (Fialko & Pearse 2012).

In this view, the flat-topped roof is merely to be understood as the roof of a much larger diapir-like magma reservoir rising from the ULVZ (Fig. 10). Understanding the geometry and thickness of the magma chamber roof is of relevance for the understanding of the structural formation of calderas, their unrest and arrest (Scandone & Acocella 2007).

4.1.4 Timing

The stress changes and the effects on the Uturuncu magmatic and fluid system may occur in association with short-term processes such as tectonic earthquakes (Jay *et al.* 2012). In addition, we propose that these changes and their effects may occur in association with long-term magmatic forcing. In addition, the contribution of a regional tectonic stress may also cause or contribute to the pattern of fractures and magma intrusions (Ruch & Walter 2010).

Inflation of the reservoir is active now, and revealed by numerous geodetic studies (McNutt *et al.* 2003; Pritchard & Simons 2004; Sparks *et al.* 2008; Hickey *et al.* 2013). We note, however, that the timing of the lineaments is not determined by us. Lineaments may occur anytime during a geological history (Ramli *et al.* 2010). At Uturuncu, the lineaments may have occurred during deflation many thousands of years ago, or during a much more recent episode. The lineaments may have formed during a single episode, distinguished pulses, or as a result of a sustained process. All this remains to be investigated.

Assuming that the models explain the data correctly, the same mid crustal region may be subject to episodes of deflation and inflation, possibly indicating longevity of a magma reservoir. Long-lived magma chambers are known to play a major role in shaping the Earth's crust, only some of these chambers lead to an eruption. A low crustal melt flux is known as one of the most important parameters for sustaining a magma chamber and maintaining longevity (Gudmundsson 2012). Magma chambers may exist and be active for durations exceeding 1 Ma, which then requires a larger intrusion depth (∼20 km) and very slow melt flux rates on the order of 10^{-4} to 10^{-1} $m^3/m^2/yr$ (Karlstrom *et al.* 2010). Given the low inflation and uplift rates of less than 10 mm as determined by InSAR data (Fialko & Pearse 2012), the Uturuncu system may reflect a magma system with low influx, typical for stable magma chambers.

4.1.5 Tectonic control

Although the volcano system is situated within a region of major NW–SE trending tectonic structures (de Silva *et al.* 2006), the deformation pattern as constrained by InSAR suggest almost perfect circular geometry in plane view (Figs 3 and 4). This differs from other volcano systems in the Andes (Pritchard & Simons 2002), for example, where the Lastarria inflation is strongly elliptic (Ruch *et al.* 2008; Anderssohn *et al.* 2009) and associated with a horizontal compressive stress field (Ruch & Walter 2010). The Uturuncu system, in turn, does currently not show such a significant tectonic stress component influence, which is in agreement with the observation elsewhere that pluton growth and size often appear independent of the tectonic setting (Cruden & McCaffrey 2001).

A tectonic control may be given in the short term. Changes in the tectonic framework, for example due to earthquakes (Walter & Amelung 2007), may abruptly change the stability and development of the Uturuncu system. Indeed, an earthquake in 2010 triggered

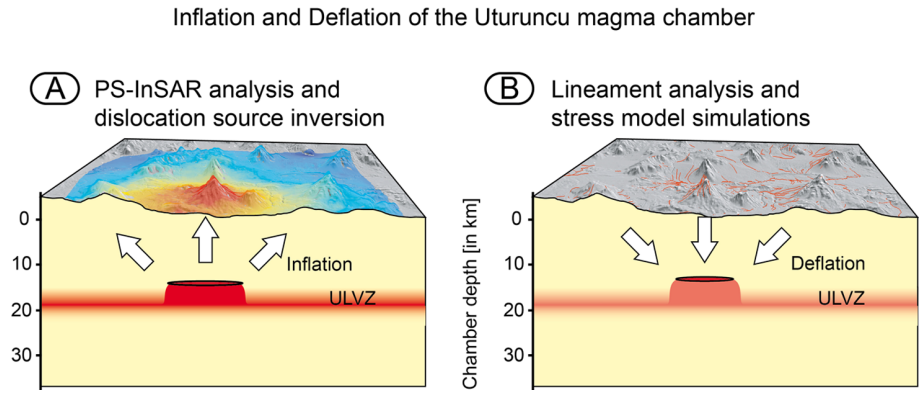

Figure 10. Synthesis of the results. Lineament analysis and stress models suggest a flat-topped deflating magma body. Note the morphologic depression of the plain surrounding Uturuncu volcano. InSAR time-series analysis shows near field uplift that is explained by an inflating flat-topped magma body. Both data can hence be explained by a flat-topped magma reservoir located close to the ultralow velocity zone (ULVZ) as determined from seismic studies (Leidig & Zandt 2003; Zandt *et al.* 2003). Far-field data requires a more prolate source (Fialko & Pearse 2012), which is conceptually illustrated here with a flat top. Not to scale.

local activity changes at Uturuncu (Jay *et al.* 2012), leaving room for speculation what could happen if an megathrust earthquake in the much closer northern Chilean subduction zone will occur—a region that has been identified as a seismic gap (Métois *et al.* 2013).

4.2 Limitations

This study builds up on many previous studies that have shown that lineaments are associated to the hidden architecture of the rock basement (Hobbs 1904), which represents the near-surface fracture network (Morelli & Piana 2006). Although the mapped lineaments may result from different geomorphological and geological processes, the structural interpretation is the most common one. However, we cannot dismiss a possible association with the lithology, foliation and bedding trends, as well as topography and loading related processes such as gravity spreading (Walter *et al.* 2006). Uturuncu is surrounded by other volcanic edifices, pyroclastic and redeposited materials, which in addition may display internal layering and provide lithologic contrast. These may have contributed to some of the lineaments mapped by us.

The lineament study assumes a simple fracture criterion that the lineaments are controlled by the maximum horizontal tensile stress. Whether the lineaments are indeed extensional in origin could not be explored in detail. We do not have clear evidences for lineament formation by horizontal tensile stress, however, a number of hints guided our interpretation in this direction. First, the lineaments at Uturuncu are mostly the negative type, which are characteristic for joints, faults and shear zones (Ramli *et al.* 2010). Secondly, by satellite data we could not observe any shear indicators on the ground associated with the lineaments, which suggests that there is not a significant horizontal, dextral or sinistral component. Thirdly, we could not identify the conjugate fracture populations that better constrain the principal stress components. Fourthly, the bulk of the lineaments was found in a moat, i.e. a morphologic depression encircling Uturuncu volcano (Fig. 10), arguing for a tensile region and against a thrust mechanism. Therefore, the fractures can be assumed to be a surface expression of an extensional stress field. It remains speculative whether these fractures are associated to normal faults at depths. We note, that, if the lineaments would be associated to a compressive stress field, their pattern and appearance could have been well simulated with a flat-topped reservoir subject to inflation, with similar geometry and located at similar depths as the aforementioned deflation source. Therefore, future studies are necessary to determine the age and nature of the lineaments, which is very crucial for understanding the development of the Uturuncu volcano system.

Other necessary simplifications may have biased the presented results. Our InSAR data set is relatively small. Recent studies (Fialko & Pearse 2012; Henderson & Pritchard 2013; Pearse & Lundgren 2013) in the Andes showed that having both ascending and descending track InSAR data allow to constrain a source with more confidence. Therefore a more complete compilation of InSAR data may certainly further improve the models and the depth resolution.

The material heterogeneities were not considered, and the Earth's surface was simulated as a flat plane. These assumptions may affect the deformations and the stress distributions, as suggested by theoretical modelling and field observations (Williams & Wadge 2000; Gudmundsson & Brenner 2004). In fact, the observed deformation field at Uturuncu may appear wider and more pronounced in the lateral extent if a layered medium is considered instead of the simple elastic half-space solutions that we described.

Because each used modelling methodology has limitations regarding the source location, geometry and strength (Dzurisin 2007). By treating the solutions in a hybrid method, we can develop a unifying conceptual model. This problem we attempt to address by comparing solutions from deformation modelling and from stress field modelling of lineaments.

None of our models consider time dependent rheologies. As (de-)pressurized magma chambers induce a stress transfer that may rupture its walls, an important relaxation process may occur in the viscoelastic shell surrounding chambers (Jellinek & DePaolo 2003), however. Therefore including more realistic rheologies may significantly help to improve our understanding of the Uturuncu magma body.

The Uturuncu case might be a rare example or a common scenario because many other volcano systems are similarly surrounded by fracture girdle(s). The general application and the validity of the described approach must be explored for more cases. Therefore, although significant knowledge has been accumulated on the activity at Uturuncu, the magma source remains to be investigated with more independent observations, where similar deformation patterns elsewhere may help further testing our current models.

5 CONCLUSIONS

The analyses of the lineaments, the stress models and the InSAR data suggest a flat-topped magma body roof under the Uturuncu volcano. Although the lineament mapping and their stress field simulation in the stress field models suggest a deflating magma body, the InSAR time-series data show an uplift and suggest an inflating magma body at the same depth. Because the location and the flat-topped geometry are consistent using both methodologies, we conjecture that the Uturuncu volcano is subject to episodic subsidence and tumescence.

ACKNOWLEDGEMENTS

The authors appreciate constructive reviews by Paul Lundgren, an anonymous reviewer and the editor, who significantly helped to improve the work. We thank Andy Hooper for his technical support and advice during our data processing and analysis using StaMPS/MTI software. Financial support was provided by the German Research Foundation (DFG MO 1851/1-1 and WA 1642/4-1), category-1 projects that were supported by the European Space Agency (3455, 3589, 2892 and AOALO3740), and the Helmholtz Alliance: Remote Sensing and Earth System Dynamics, supported in the frame of the Initiative and Network Fund of the Helmholtz Association.

REFERENCES

Allmendinger, R.W., Jordan, T.E., Kay, S.M. & Isacks, B.L., 1997. The evolution of the Altiplano-Puna Plateau of the Central Andes, *Ann. Rev. Earth planet. Sci.,* **25,** 139–174.

ANCORP Working Group, 2003. Seismic imaging of a convergent continental margin and plateau in the central Andes (Andean Continental Research Project 1996 (ANCORP'96)), *J. geophys. Res.,* **108**(B7), 2328, doi:10.1029/2002JB001771.

Anderson, E.M., 1951. *The Dynamics of Faulting and Dyke Formation, with Applications to Britain*, Oliver and Boyd, 206 pp.

Anderssohn, J., Motagh, M., Walter, T.R., Roseneau, M., Kaufmann, H. & Oncken, O., 2009. Surface deformation time series and source modeling for a volcanic complex system based on satellite wide swath and image mode interferometry: the Lazufre system, central Andes, *Remote Sens. Environ.,* **113,** 2062–2075.

Arellano-Baeza, A.A., Zverev, A.T. & Malinnikov, V.A., 2006. Study of changes in the lineament structure, caused by earthquakes in South America by applying the lineament analysis to the Aster (Terra) satellite data, *Adv. Space Res.,* **37,** 690–697.

Berardino, P. *et al.*, 2002. Evidence for a peculiar style of ground deformation of Vesuvius Volcano revealed by 10 years of ERS mission, in *Proceedings of the Remote Sensing; Integrating our View of the Planet,* Institute of Electrical and Electronics Engineers, New York, NY, USA, pp. 3614–3616.

Bergantz, G.W., 2000. On the dynamics of magma mixing by reintrusion: Implications for pluton assembly processes, *J. Struct. Geol.y,* **22,** 1297–1309.

Bott, M.H. & Smithson, S.B., 1967. Gravity investigations of subsurface shape and mass distributions of granite batholiths, *Bull. Geol. Soc. Am.,* **78,** 859–878.

Chmielowski, J., Zandt, G. & Haberland, C., 1999. The central Andean Altiplano-Puna magma body, *Geophys. Res. Lett.,* **26**(6), 783–786.

Cruden, A.R. & McCaffrey, K.J.W., 2001. Growth of plutons by floor subsidence; implications for rates of emplacement, intrusion spacing and melt-extraction mechanisms, *Phys. Chem. Earth Part A: Solid Earth Geod.,* **26**(4–5), 303–315.

de Silva, S.L., 1989. Altiplano-Puna volcanic complex of the Central Andes, *Geology (Boulder),* **17**(12), 1102–1106.

de Silva, S.L. & Francis, P.W., 1991. *Volcanoes of the Central Andes*, Springer-Verlag, 216 pp.

de Silva, S.L. & Gosnold, W.D., 2007. Episodic construction of batholiths; insights from the spatiotemporal development of an ignimbrite flare-up, *J. Volc. Geotherm. Res.,* **167**(1–4), 320–335.

de Silva, S., Zandt, G., Trumbull, R., Viramonte, J.G., Salas, G. & Jimenez, N., 2006. Large ignimbrite eruptions and volcano-tectonic depressions in the Central Andes: a thermomechanical perspective, *Geol. Soc. Specl. Publ.,* **269,** 47–63.

Dzurisin, D., 2007. *Volcano Deformation: Geodetic Monitoring Techniques*, Praxis Publishing, 441 pp.

Faeghlashgary, P., Motagh, M., Sharifi, M.A. & Saradjian, M.R., 2012. Source parameters of the September 10, 2008 Qeshm Earthquake in Iran inferred from the Bayesian Inversion Envisat and ALOS InSAR Observations, in *VII Hotine-Marussi Symposium on Mathematical Geodesy: Proceedings of the Symposium in Rome,* International Association of Geodesy Symposia, Vol. 137, pp. 319–325, eds Sneeuw, N., Novak, P., Crespi, M. & Sansò, F., 6–10 June 2009, Springer.

Fialko, Y., Khazan, Y. & Simons, M., 2001. Deformation due to a pressurized horizontal circular crack in an elastic half-space, with applications to volcano geodesy, *Geophys. J. Int.,* **146**(1), 181–190.

Fialko, Y. & Pearse, J., 2012. Sombrero uplift above the Altiplano-Puna Magma body: evidence of a ballooning mid-crustal diapir, *Science,* **338**(6104), 250–252.

Gudmundsson, A., 2012. Magma chambers: Formation, local stresses, excess pressures, and compartments, *J. Volc. Geotherm. Res.,* **237–238,** 19–41.

Gudmundsson, A. & Brenner, S.L., 2004. Local stresses, dyke arrest and surface deformation in volcanic edifices and rift zones, *Ann. Geophys.,* **47**(4), 1433–1454.

Hancock, P.L. & Al-Kadhi, A., 1978. Analysis of mesoscopic fractures in the Dhruma-Nisah segment of the Central Arabian Graben System, *Geol. Soc. Lond.,* **135,** 339–347.

Henderson, S.T. & Pritchard, M.E., 2013. Decadal volcanic deformation in the Central Andes Volcanic Zone revealed by InSAR time series, *Geochem. Geophys. Geosyst.,* **14**(5), 1358–1374.

Hickey, J., Gottsmann, J. & del Potro, R., 2013. The large-scale surface uplift in the Altiplano-Puna region of Bolivia: A parametric study of source characteristics and crustal rheology using finite element analysis, *Geochem. Geophys. Geosyst.,* **14**(3), 540–555.

Hobbs, W.H., 1904. Lineaments of the Atlantic border region, *Geol. Soc. Am. Bull.,* **15,** 483–506.

Hooper, A., 2008. A multi-temporal InSAR method incorporating both persistent scatterer and small baseline approaches, *Geophys. Res. Lett.,* **35,** L16302, doi:10.1029/2008GL034654.

Jay, J.A. *et al.*, 2012. Shallow seismicity, triggered seismicity, and ambient noise tomography at the long-dormant Uturuncu Volcano, Bolivia, *Bull. Volcanol.,* **74**(4), 817–837.

Jellinek, A.M. & DePaolo, D.J., 2003. A model for the origin of large silicic magma chambers: Precursors of caldera-forming eruptions, *Bull. Volcanol.,* **65**(5), 363–381.

Karlstrom, L., Dufek, J. & Manga, M., 2010. Magma chamber stability in arc and continental crust, *J. Volc. Geotherm. Res.,* **190**(3–4), 249–270.

Leidig, M. & Zandt, G., 2003. Modeling of highly anisotropic crust and application to the Altiplano-Puna volcanic complex of the central Andes, *J. geophys. Res.,* **108**(B1), 2014, doi:10.1029/2001JB000649.

Marsh, B.D., 1982. On the mechanics of igneous diapirism, stoping, and zone melting, *Am. J. Sci.,* **282**(6), 808–855.

Marsh, B.D., 2000. Magma chambers, in *Encyclopedia of Volcanoes*, Academic Press, pp. 191–206.

McNutt, S.R. & Pritchard, M.E. Anonymous, 2003. Seismic and Geodetic Unrest at Uturuncu Volcano, Bolivia, in *Proceedings of the American Geophysical Union, Fall Meeting,* AGU.

Métois, M., Vigny, C., Socquet, A., Delorme, A., Morvan, S. & Ortega, I., 2013. GPS-derived interseismic coupling on the subduction and seismic hazards in the Atacama region, Chile, *Geophys. J. Int.,* **194**(3), 1283–1294.

Mogi, A., 1958. Relations between the eruptions of various volcanoes and the deformations of the ground surfaces around them, *Bull. Earthq. Res. Inst. Univ. Tokyo,* **36,** 99–134.

Morelli, M. & Piana, F., 2006. Comparison between remote sensed lineaments and geological structures in intensively uncultivated hills, *Int. J. Remote Sens.,* **26**(7), 1463–1475.

Okada, Y., 1992. Internal deformation due to shear and tensile faults in a half-space, *Bull. seism. Soc. Am.,* **82**(2), 1018–1040.

O'Leary, D.W., Friedman, J.D. & Pohn, H.A., 1976. Lineament, linear, lineation: some proposed new standards for old terms, *Bull. Geol. Soc. Am.,* **87,** 1463–1469.

Oncken, O., Hindle, D., Kley, J., Elger, K., Victor, P. & Schemmann, K., 2006. Deformation of the Central Andean upper plate system—facts, fiction, and constraints for plateau models, in *The Andes—Active Subduction Orogeny*, pp. 3–27, eds Oncken, O., Chong, G., Franz, G., Giese, P., Götze, H.-J., Ramos, V., Strecker, M., & Wigger, P., Springer.

Pearse, J. & Lundgren, P., 2013. Source model of deformation at Lazufre volcanic center, central Andes, constrained by InSAR time series, *Geophys. Res. Lett.,* **40,** 1059–1064.

Petford, N., Cruden, A.R., McCaffrey, K.J.W. & Vigneresse, J.L., 2000. Granite magma formation, transport and emplacement in the Earth's crust, *Nature,* **408,** 669–673.

Pitcher, W.S., 1979. The nature, ascent and explacement of granitic magmas, *J. geol. Soc. Lond.,* **136,** 627–662.

Pritchard, M.E. & Simons, M., 2002. A satellite geodetic survey of large-scale deformation of volcanic centres in the central Andes, *Nature,* **418**(6894), 167–171.

Pritchard, M.E. & Simons, M., 2004. An InSAR-based survey of volcanic deformation in the central Andes, *Geochem. Geophys. Geosyst.,* **5,** Q02002, doi:10.1029/2003GC000610.

Pritchard, M.E., Simons, M., Rosen, P.A., Hensley, S. & Webb, F.H., 2002. Co-seismic slip from the 1995 July 30 M (sub w) = 8.1 Antofagasta, Chile, earthquake as constrained by InSAR and GPS observations, *Geophys. J. Int.,* **150**(2), 362–376.

Ramli, M., Yusof, N., Yusoff, M., Juahir, H. & Shafri, H., 2010. Lineament mapping and its application in landslide hazard assessmenta review, *Bull. Eng. Geol. Environ.,* **69,** 215–233.

Riller, U. & Oncken, O., 2003. Growth of the Central Andean Plateau by tectonic segmentation is controlled by the gradient in crustal shortening, *J. Geol.,* **111**(3), 367–384.

Ruch, J. & Walter, T.R., 2010. The relationship between current uplift geometry revealed by InSAR, structural framework, and the present-day stress field at Lazufre volcanic area, central Andes, *Tectonophysics,* **492,** 133–140.

Ruch, J., Anderssohn, J., Walter, T.R. & Motagh, M., 2008. Caldera-scale inflation of the Lazufre volcanic area, South America; evidence from InSAR, *J. Volc. Geotherm. Res.,* **174**(4), 337–344.

Scandone, R. & Acocella, V., 2007. Control of the aspect ratio of the chamber roof on caldera formation during silicic eruptions, *Geophys. Res. Lett.,* **34**(22), L22307, doi:10.1029/2007GL032059.

Schmitz, M., Heinsohn, W.D. & Schilling, F.R., 1997. Seismic, gravity and petrological evidence for partial melt beneath the thickened Central Andean crust (21–23 degrees S), *Tectonophysics,* **270**(3–4), 313–326.

Shirzaei, M. & Walter, T.R., 2009. Randomly iterated search and statistical competency as powerful inversion tools for deformation source modeling: Application to volcano interferometric synthetic aperture radar data, *J. geophys. Res.-Solid Earth,* **114**, doi:10.1016/j.epsl.2012.04.001.

Soto-Pinto, C., Arellano-Baeza, A. & Sánchez, G., 2012. A new code for automatic detection and analysis of the lineament patterns for geophysical and geological purposes (ADALGEO), *Comput. Geosci.,* **57,** 93–103.

Sparks, R.S.J., Folkes, C.B., Humphreys, M.C.S., Barfod, D.N., Clavero, J., Sunagua, M.C., McNutt, S.R. & Pritchard, M.E., 2008. Uturuncu Volcano, Bolivia; volcanic unrest due to mid-crustal magma intrusion, *Am. J. Sci.,* **308**(6), 727–769.

Thomas, A.L., 1993. Poly3D: a three-dimensional, polygonal element, displacement discontinuity boundary element computer program with applications to fractures, faults, and cavities in the Earth's crust, *MS thesis,* Stanford University, Stanford, CA, pp. 221.

Twiss, R.J. & Moores, E.M., 1992. *Structural Geology,* W.H. Freeman and Company, 532 pp.

Usai, S. *et al.*, 2003. MINERVA; an INSAR monitoring system for volcanic hazard, in *Proceedings of the 2003 IEEE International Geoscience and Remote Sensing Symposium, IGARSS 2003: Learning from Earth's Shapes and Sizes,* Institute of Electrical and Electronics Engineers, New York, NY, United States, pp. 2433–2435.

Walker, G.P.L., 1989. Gravitational (density) controls on volcanism, magma chambers and intrusions, *Aust. J. Earth Sci.,* **36**(2), 149–165.

Walter, T.R., 2007. How a tectonic earthquake may awake silent volcanoes: stress triggering during the 1996 earthquake–eruption sequence at the Karymsky Volcanic Group, Kamchatka, *Earth planet. Sci. Lett.,* **264**(3–4), 347–359.

Walter, T.R. & Amelung, F., 2007. Volcanic eruptions following M>9 megathrust earthquakes: Implications for the Sumatra-Andaman volcanoes, *Geology,* **35**(6), 539–542.

Walter, T.R., Klugel, A. & Munn, S., 2006. Gravitational spreading and formation of new rift zones on overlapping volcanoes, *Terra Nova,* **18**(1), 26–33.

Williams, C.A. & Wadge, G., 2000. An accurate and efficient method for including the effects of topography in three-dimensional elastic models of ground deformation with applications to radar interferometry, *J. geophys. Res., B, Solid Earth Planets,* **105**(4), 8103–8120.

Yun, S., Segall, P. & Zebker, H., 2006. Constraints on magma chamber geometry at Sierra Negra Volcano, Galapagos Islands, based on InSAR observations, *J. Volc. Geotherm. Res.,* **150**(1–3), 232–243.

Zandt, G., Leidig, M., Chmielowski, J., Baumont, D. & Yuan, X., 2003. Seismic detection and characterization of the Altiplano-Puna magma body, Central Andes, *Pure appl. Geophys.,* **160**(3–4), 789–807.